D. W. Pohl

Forced Rayleigh Scattering

Forced Rayleigh scattering (FRS) is a light scattering technique used to investigate light-induced grating structures that decay in a relaxational or almost relaxational manner. Such gratings can be created by interference and absorption of two pump beams and probed by a third beam, usually of different frequency. They may consist of spatially varying excited state populations with picosecond lifetimes or of long-lived variations in temperature, composition, and/or density. Forced Rayleigh scattering provides high sensitivity with respect to the amplitude and dynamics of such gratings and allows investigations not accessible by classical scattering techniques. The principles, techniques, and applications of FRS are reviewed.

Introduction

A number of experiments on thermal and thermodynamic properties of matter have recently been performed using the technique of forced Rayleigh scattering (FRS). To a large extent, these investigations deal with thermodynamic quantities and their transport properties, such as heat diffusion in solids [1-3] and liquids [2] (particularly in liquid crystals where strong anisotropy is found [4]); second sound (wavelike propagation of heat) in crystals [5]; coupling between heat and mass diffusion in lipid water solutions [6] and in binary mixtures [7]; and "critical slowing-down" near a convective instability [8]. These phenomena involve the excitation of modes that are close to the mean thermal energy, *i.e.*, close to thermal equilibrium. They usually take place on a fairly slow time scale and may be defined as FRS in the "strict" sense.

A second line of investigation concerns electronic excitations and their decay, recombination, and charge transfer [9-14]. Here, the time constants may vary between years (photochromism) and fractions of a picosecond. These excitations are far from thermal equilibrium.

Both the experimental requirements and the physical background are quite different in these two fields of FRS activity. In this paper FRS is first described and discussed with respect to applications close to thermal equilibrium that are related to heat transport. The sensitivity, technical requirements, and limitations of this technique are then evaluated and related to classical Rayleigh scattering (CRS) [15]. Finally, other thermodynamic quantities and FRS far from thermal equilibrium are discussed.

Rayleigh scattering (RS) originally referred to the scattering of light by atmospheric molecules and their fluctuating density [16]. The frequency of light is essentially unaffected in this process; the scattering is *elastic* and *quasi-elastic* (very small shifts admitted). A variety of other mechanisms of quasi-elastic scattering have since been discovered. If the processes involved are purely diffusive or relaxational, the decay is exponential, and the frequency spectrum consists of one or more Lorentzians centered around the incident frequency. Physical quantities of this type are density, temperature, strain, certain components of the stress tensor, concentration (mass), orientation of molecular units, internal and free energy, chemical potential, and entropy. In general, some of these quantities are coupled to one another, *e.g.*, density, temperature and entropy which form the well-known isobaric entropy fluctuations in gases and liquids. Under certain circumstances, some of these processes, such as the transport of heat (second sound) or the composition of a mixture (chemical waves), may become (marginally) wavelike. The corresponding spectrum has resolvable components offset from the incident frequency [17] and resembles Brillouin scattering (BS).

Copyright 1979 by International Business Machines Corporation. Copying is permitted without payment of royalty provided that (1) each reproduction is done without alteration and (2) the *Journal* reference and IBM copyright notice are included on the first page. The title and abstract may be used without further permission in computer-based and other information-service systems. Permission to *republish* other excerpts should be obtained from the Editor.

Classical and forced Rayleigh scattering

• *Coupling coefficients*

The basic requirement for a fluctuation to cause observable light scattering is some amount of coupling to the electric susceptibility at optical frequencies, *i.e.*, to the refractive index. Variations δn both in the real and imaginary parts of the refractive index can contribute. Close to $k_B T$ (k_B = Boltzmann constant), however, the change is restricted to the real part in most experiments. The minimum coupling strength required depends on the level of stray light reaching the detector and on the intensity of the light source.

To illustrate this problem, the thermo-optic coefficient $(\partial n/\partial T)_{eff}$ responsible for scattering by temperature fluctuations is considered, where n and T denote refractive index and temperature; the subscript eff refers to the constraints imposed on the derivative for physical and geometrical reasons [18].

Sodium fluoride was chosen as an example; its thermo-optic coefficients have been determined over a large temperature interval [19]. The coefficient of linear thermal expansion α_ℓ and the isobaric coefficient $(\partial n/\partial T)_p$ are roughly proportional to T^3, but the temperature dependence of $(\partial n/\partial T)_{eff}$ is more complicated because of a cancellation between elasto-optic and isochoric thermo-optic contributions.

• *Classical Rayleigh scattering and its limitations*

Classical low-energy light scattering techniques are based on statistical thermodynamic fluctuations. Discrimination against stray light is the dominant problem in RS because of the small frequency shifts involved. For this reason, CRS has thus far found only limited application in contrast to Brillouin and Raman scattering techniques.

The CRS rate (per unit volume and solid angle; forward direction) expected on the basis of $\partial n/\partial T$ is shown in Fig. 1, which is taken from Ref. [19]. Curves 1 (effective Rayleigh scattering rate) are obtained from $(\partial n/\partial T)_{eff}$, the specific heat C_p, the volume V (= 1 cm^3), and the mean square temperature fluctuation [20]

$$\langle \Delta T^2 \rangle = k_B T^2/\rho C_p V, \qquad (1)$$

where ρ is the density. The corresponding scattering rate calculated from the theory of Landau and Placzek [21], which takes into account only the influence of thermal expansion, is also shown (curve 2), along with the Brillouin scattering (curve 3).

It is to be noted that classical scattering rates always refer to intensities because of the random nature of the fluctuations, even if homo- or heterodyne techniques are used [15]. The CRS rate is therefore proportional to $(\partial n/\partial T)^2_{eff}$. The mean square temperature fluctuation is approximately proportional to T^5; it decays from 10^{-11} per steradian at room temperature to $<10^{-17}$ per steradian around 20 K. The rate of BS, introduced in Fig. 1 for comparison, is related to linear properties of the lattice. The coupling is practically independent of T. The scattering rate is proportional to the adiabatic density fluctuation $\langle \Delta\rho^2 \rangle \propto T$ and hence is much easier to follow down to cryogenic temperatures.

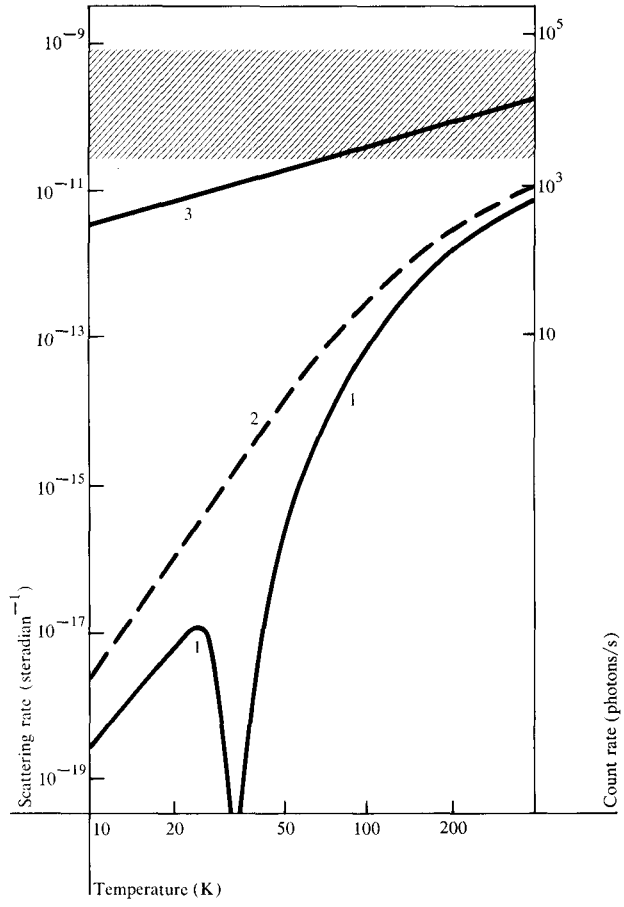

Figure 1 Classical scattering rates (from Ref. [19]) for a typical NaF crystal and the estimated count rates under second sound conditions. Curves 1 give the effective Rayleigh scattering; curve 2, the scattering expected from Landau-Placzek theory; and curve 3, the Brillouin scattering.

Figure 1 also shows a level of shot noise that is estimated from an incident laser power of 300 mW, an acceptance angle of 10^{-4} steradian, and a conversion efficiency into stray light on the order of 10^{-7}. These data refer to the experimental requirements for the detection of second sound by means of CRS. Second sound is bound

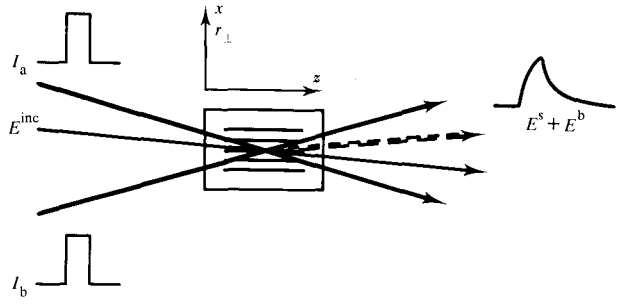

Figure 2 A schematic of the FRS experiment. The I_a and I_b pump beams are from the same source and are frequently rectangular pulses produced by a chopper. Here, E^{inc}, E^s, and E^b refer to the incident probe beam and the scattered and stray radiation, respectively (E^b often acts as a local oscillator for heterodyne detection).

to a certain interval of wavelengths, the so-called window condition [22, 23], and requires very small scattering angles. For this reason, a large stray light level and a small acceptance had to be chosen for these experiments. Since second sound in NaF is not expected to exist much above 25 K, CRS can be clearly ruled out for signal-to-noise considerations. It was this negative outcome [19] which led us to the concept of FRS as an extremely sensitive scattering technique [1]. About the same time as these experiments on second sound, Eichler and coworkers independently developed FRS for determination of heat conductivity in liquids and solids [2]. Precursors to the FRS technique can be seen in stimulated Rayleigh scattering [24] and self-diffraction [25].

• *Principle of FRS*

The concept of forced Rayleigh scattering is to replace the statistical, weak, and random fluctuations utilized in CRS with driven, strong, and coherent excitations [1, 2]; scattering from the latter "fluctuations" is orders of magnitude greater than CRS and has a well-defined phase. Moreover, it is more easily discriminated from stray light, since the driven or "forced" excitation can be modulated; this allows the use of lock-in detection methods. The requirements on alignment, however, are considerably more demanding for FRS than for CRS. The data available from the two scattering techniques are closely related but not identical. Classical Rayleigh scattering provides correlations of the type $\langle \Delta S(t, q)\ \Delta S(t + \tau, q)\rangle$ [15], while FRS directly yields the dynamics of $\Delta S(t, q)$. Here ΔS, t (τ), q, and Ω denote fluctuation amplitude, time, wave vector of the Fourier component under consideration, and frequency, respectively.

To excite such a fluctuation in a well-defined way, an interference pattern is created in the bulk or at the surface of the sample by irradiation with a pump laser. The shape of the pattern is widely variable and may be adjusted for the particular purpose. In general, plane gratings are used. For this purpose, two collimated beams (usually from the same source) are made to intersect at the sample (Fig. 2). The q-vector of the fluctuation is then determined by the angle θ between the pump beams and their wave vectors $\vec{k}_{a,b}(|k_a| = |k_b| = k_p)$,

$$q = |\vec{q}| = |\vec{k}_a - \vec{k}_b| = 2k_p \sin \theta/2. \tag{2}$$

The absorption process primarily excites electronic or vibrational states far above the thermal energy $k_B T_0$, where T_0 is the average temperature. These states typically decay on a subpicosecond to nanosecond time scale (*cf.* "high" energy FRS). The resulting heat/temperature pattern, in general, has the same wave vector $\vec{q}$. In most cases, the amplitude $\delta T << T_0$. The decay time depends on the value of q and is usually in the microsecond to millisecond range. The temperature pattern may, in a further process, shift chemical equilibria, cause changes in the concentration of mixtures, or influence the boundary between two phases. Such secondary thermodynamic fluctuations are spatially modulated with the wave vector $\vec{q}$, but typically decay even slower than thermal fluctuations.

The forced excitation is detected by a third laser beam of different frequency, which is adjusted to meet the Bragg condition with respect to $\vec{q}$. The scattered light travels exactly in the complementary Bragg direction, restricting the angle of acceptance to diffraction-limited conditions. Thus, the level of stray light can be kept quite low.

Theoretical and technical considerations

• *Thermal gratings*

Thermal gratings are the most common and almost inevitable result of irradiation of the sample by an interference pattern. Other types of gratings respond and relax quite similarly to thermal ones, which were therefore chosen as the example gratings.

The dynamics of thermal gratings are governed by the equation of heat diffusion supplemented by a driving term that accounts for the absorbed pump radiation:

$$\dot{T} = \nabla \cdot \chi(T) \nabla T + [\alpha(I_a I_b)^{1/2}/\rho C_p] \cos(\vec{q} \cdot \vec{r}). \tag{3a}$$

Equation (3a) in general can be simplified to

$$\dot{T} = \chi \nabla^2 T + [\alpha(I_a I_b)^{1/2}/\rho C_p] \cos(\vec{q} \cdot \vec{r}). \tag{3b}$$

The thermal diffusivity χ is given by $K/\rho C_p$, where K is the heat conductivity; α is the absorption coefficient at

the frequency of the pump beams, I_a and I_b are the respective beam intensities, $\vec{r}$ is the spatial coordinate, ∇ is the gradient operator, $\nabla \cdot \chi$ is the divergence of χ, and ∇^2 is the Laplacian operator. The temperature dependence of χ can usually be neglected but does need to be considered close to a phase transition and at very low temperatures. Further, K and χ are second-rank tensors. They are degenerate, however, in cubic and disordered media, and in these cases, the simpler Eq. (3b) can be used, as in the following discussion.

Equation (3b) has the simple *plane wave solution* if the extension of the grating is large compared to the fringe spacing $2\pi/q$. To satisfy this condition, the spot size w_p of the pump beams has to be large ($w_p q >> 1$) and the absorption small ($\alpha/q << 1$). We may then set I_a and I_b constant with respect to $\vec{r}$ and

$$T(\vec{r}, t) = T_0 + \delta T(t) \cos(\vec{q} \cdot \vec{r}). \tag{4}$$

Equations (3b) and (4) yield, for the time dependence of δT,

$$\dot{\delta T} - \chi q^2 \delta T = \alpha (I_a I_b)^{1/2} / \rho C_p. \tag{5}$$

The steady state amplitude is

$$\delta T_{st} = \alpha (I_a I_b)^{1/2} / K q^2. \tag{6}$$

Note that δT_{st} is independent of ρC_p (which enters at nonstationary conditions only). In order to obtain large δT, a small grating constant, *i.e.*, a small scattering angle θ, is favorable. In fact, scattering in the forward direction has been utilized in most experiments on FRS so far, sometimes with scattering angles as small as a few milliradians. In a typical experiment δT_{st} would be 1 to 10 mK, as compared with statistical fluctuations on the order of 10 nK, which are responsible for CRS. This latter statistical fluctuation refers to an ambient temperature of 300 K and a volume of 0.1 cm^3.

If the pump radiation is suddenly turned on (*i.e.*, a step function), δT lags behind with a relaxation time

$$\tau = 1/\chi q^2 \tag{7}$$

and

$$\delta T = \delta T_{st}[1 - \exp(-t/\tau)]. \tag{8}$$

The corresponding exponential decay occurs after turnoff. Thus, by recording the temporal dependence of the scattering, the thermal diffusivity can be determined immediately, sensitively, and in a contact-free manner.

The response to a short pump pulse with duration $t_p << \tau$ is

$$\delta T_p = [\alpha (I_a I_b)^{1/2} t_p / \rho C_p] \exp(-t/\tau), \tag{9}$$

which allows K and C_p to be determined separately if I_a and I_b are known with sufficient accuracy.

Amplitude modulation of the pump with frequency $\Omega/2\pi$ results in a square root of a Lorentzian for δT:

$$|\delta T(\Omega)| = \delta T_{st}(1 + \Omega^2 \tau^2)^{-1/2} \tag{10}$$

Equation (10), except for the exponent 1/2, is identical to the thermal CRS spectrum.

Equations (3) through (10) need considerable modification in the *second-sound regime*. Equation (3) is to be supplemented by a second time derivative in T requiring a (damped) wavelike solution. As a result, the temperature response to pump modulation has a resonance at the second-sound frequency $\Omega_0 = q c_0$ (c_0 = speed of second sound);

$$|\delta T(\Omega)| = \delta T_0 \Gamma_R [(\Omega - \Omega_0)^2 + \Gamma_R^2]^{-1/2}. \tag{10a}$$

Here Γ_R accounts for damping (see the insert to Fig. 3), which is closely related to the probability of inelastic phonon scattering.

The effect of finite spot size w_p can be accounted for in the solution of Eq. (3b) by Fourier transformation of the pump intensity distribution and superposition of the resulting $\delta T(\tilde{q})$. The dominant contribution comes from $\tilde{q} \leq \pi/w_p^2$, which decays with a typical time constant of

$$\tilde{\tau} \approx w_p^2 / \pi^2 \chi. \tag{11}$$

This decay is slow ($\tilde{\tau} >> \tau$) and has frequently been observed in FRS. It can be quite disturbing if another grating-related slow effect is to be observed. However, a check is easily made by reversing the phase of the thermal grating; this also reverses the phase of a grating-produced signal [1, 6] but not of one caused by a finite spot-size effect. An elegant way of completely eliminating the latter contribution is to periodically reverse both the grating phase and the received signal. Integration with a signal averager then yields the pure grating signal [6].

A fairly simple analytic solution to Eq. (3b) also exists for strong absorption with $I_{a,b}(r_\perp, z) = I_0(r_\perp) \exp(-\alpha z)$ (for the coordinates, see Fig. 2) and short pulse excitation. The product ansatz for the temperature

$$T = T_\perp(r_\perp, t) g(z, t) \tag{12}$$

allows a separation that yields for $T_\perp$ the plane wave solution just discussed. The explicit form of $g(z, t)$, a combination of exponentials and erfc functions, represents the temperature response to absorption of an unmodulated plane wave but is of minor importance here.

• *Stress, strain, and refractive-index grating*

Thermal fluctuations in liquids and gases can be separated into isentropic sound waves and isobaric entropy fluctuations. In solids [18], entropy fluctuations are isobaric only with respect to the stress component parallel to $\vec{q}$. In the simplest case, an amorphous substance or cubic crystal with the $\langle 100 \rangle$ direction parallel to $\vec{q}$ and $\vec{x}$, the amplitudes of the stress $\overleftrightarrow{\sigma}$ and strain $\overleftrightarrow{u}$ gratings associated with δT are

$$\sigma_{yy} = \sigma_{zz} = \alpha_{\text{eff}}(c_{12} - c_{11})\delta T \tag{13}$$

and

$$u_{xx} = \alpha_{\text{eff}}\delta T, \tag{14}$$

while all the other tensor components vanish; c_{11} and c_{12} are the elastic constants and

$$\alpha_{\text{eff}} = \alpha_{\ell}(1 + 2c_{12}/c_{11}) \tag{15}$$

is the effective or clamped thermal expansion coefficient appropriate for plane wave geometry.

The anisotropy expressed in Eqs. (13) and (14) is carried on to the refractive index grating δn associated with $\overleftrightarrow{u}$ and δT:

$$\delta n_{ij} = (\partial n_{ij}/\partial T)_{\text{eff}}\delta T = \delta_{ij}(\partial n/\partial T)_u \delta T - \frac{1}{2} n_0^3 p_{ijkl} u_{kl}(\delta T). \tag{16}$$

The first term is isotropic and represents the variation of polarizability with phonon occupation (clamped conditions). This effect was previously assumed to be negligible but Wehner and Klein [26] showed that it can actually be considerably larger than the second term. Particularly large values may be expected near a phase transition or in glasses because of structural rearrangement; this does indeed seem to be the case [27].

The second term in Eq. (16) represents the influence of thermal expansion on the refractive index. The p_{ijkl} are Pockel's elasto-optic constants and n_0 is the average refractive index. The microscopic origin of this term is seen in the variation of particle density at constant polarizability (which again yields an isotropic contribution to δn) and in the variation of polarizability a_{ij} with strain (which is anisotropic):

$$p_{ijkl} = -(2/n_0^2)[\delta_{ij}\delta_{kl} + (\partial a_{ij}/a\partial u_{kl})]. \tag{17}$$

The last term, also connected with structural rearrangement, can be separated experimentally from the others by comparison of polarized and depolarized scattering. Under certain conditions, absorption changes may also occur at the probe laser frequency; δn_{ij} is then complex. The expected scattering phenomena are quite similar to those of a pure index grating, particularly if δn_{ij} is small.

• *Scattering rate*

The simplest conditions exist for forward scattering: small absorption within the sample length ℓ and small δn_{ij}. For $\theta << 1$ one can neglect the sideways "walk-off" of the laser beams, a complication that was considered analytically by Siegmann [28]. If $\alpha\ell << 1$, δn_{ij} is spatially constant. The amplitude components of the scattered beam E_i^s are then proportional to the amplitude components of the incident beams E_j^{inc} $(i, j = x, y)$, to δn_{ij}, and to the wave vectors $k^{\text{inc}} \approx k^s$:

$$E_i^s = -ik^{\text{inc}}\ell\delta n_{ij}E_j^{\text{inc}}. \tag{18}$$

This formula is valid quite generally in the sense that δn_{ij} $(<<1)$ need not be caused by a temperature fluctuation and may even be a static quantity such as a volume hologram.

A surprisingly simple expression for the scattered amplitude also exists in the case of strong absorption at the pump laser frequency, $\alpha\ell >> 1$. Equation (18) must be replaced by the more general expression

$$E_i^s = -i\vec{k}^{\text{inc}}E^{\text{inc}}\int_0^{\ell} \delta n_{ij}(z, t)dz \approx \int_0^{\ell} g(z, t)dz. \tag{18a}$$

If the sample is isolated thermally and excited by a short pulse, advantage can be taken of the fact that $g(z, t)$ itself satisfies Eq. (3b) with zero driving force. Integration over z yields $\int_0^{\ell}\dot{g}(z, t)dz \approx 0$; therefore $\int_0^{\ell} g(z, t)dz$ is a constant. The constant longitudinal part is a manifestation of energy conservation for $q = 0$. The dynamics of the scattered signal (after the pump is turned off) therefore depends only on the transverse part of δT. The decay time, in particular, is proportional to q^{-2}, even if $\alpha/q >> 1$. This finding was confirmed in an investigation on potassium dihydrogen phosphate (KDP) with 5-μm pump radiation, where the KDP was practically opaque [27].

Detection of the scattered light may be either homodyne (direct) or heterodyne. The choice is given by the level of stray light E_i^b reaching the detector. Direct detection is most straightforward but requires $E_i^s > E_i^b$. However, quite often the scattering is weak, such that $E_i^s < E_i^b$ and even $E_i^s << E_i^b$. Detection is then necessarily heterodyne, with E_i^b as local oscillator, unless a separate source is provided. The resulting detector current is

$$i \approx |E_i^b + E_i^s|^2 \approx |E_i^b|^2 + 2E_i^s E_i^b \cos\phi, \tag{19}$$

where the second term contains the signal and ϕ refers to the phase between E^s and E^b. Thus, the sign of the signal depends on the phase of the index grating.

• *Limits of sensitivity*

Heterodyne detection is a very sensitive technique because both the received signal and the shot noise level are

proportional to E^b. (The tensorial notation is now dropped for simplicity.) Hence the signal-to-noise ratio SNR_v [defined in terms of currents (voltages), not power] depends on E^s only. Expressing E^s in terms of the (amplitude) scattering efficiency (E^s/E^{inc}) and the incident power flux P^{inc} ($\propto |E^{inc}|^2$) yields [29]:

$$SNR_v = (P^{inc}\eta/h\nu^{inc}B_D)^{1/2}(E^s/E^{inc}), \tag{20}$$

where η is the quantum efficiency of the detector, $h\nu^{inc}$ is the photon energy, and B_D is the limiting bandwidth of the detection apparatus; $SNR_v > 1$ can be easily achieved with conventional lasers, liquid or solid samples at ambient conditions, and absorption on the order of 1 cm^{-1}.

The steady state FRS rate $|E^s|/|E^{inc}|$ in NaF, calculated on the basis of reasonable experimental conditions, is shown in Fig. 3, together with the typical level of shot noise and other experimental data to be discussed later. Down to fairly low temperatures, the FRS signal is well above noise, quite in contrast to CRS (Fig. 1). The temperature dependence in the diffusive regime is given by $(\partial n/\partial T)_{eff}K(T)$.

The extreme sensitivity of FRS also becomes obvious from a determination of the minimum detectable scattering efficiency $(E^s/E^{inc})_{min}$. Putting $SNR_v = 1$, $B_D = 1$ Hz, $P^{inc} = 10$ mW at $h\nu^{inc} = 2$ eV, and $\eta = 0.2$, we find

$$(E^s/E^{inc})_{min} \approx 10^{-8} \tag{21a}$$

and

$$\delta n_{min} = 10^{-13}, \tag{21b}$$

where $\ell k^{inc} = 10^5$ has been assumed. Equations (21) provide minimum values for the various parameters entering the scattering efficiency.

In Table 1, the minimum values for the different parameters are summarized for typical or easily attainable values of the respective other quantities for solids (gases): $\alpha = 1$ cm^{-1}, $I_a = I_b = 100$ W/cm^2 for $P_a = P_b = 1$ W, area $A = 1$ mm^2, $q = 10^3$ cm^{-1}, $K = 0.1$ (3×10^{-4}) W/cm-K, and $(\partial n/\partial T)_{eff} = 10^{-5}$ (3×10^{-3}) K^{-1}.

It is seen that FRS can be used not only to study thermal excitations and their dynamics, but also to detect very small absorption at the pump frequency. Errors from surface absorption can be excluded by placing the grating zone well inside the sample. Also, FRS allows thermo-optic coefficients (and some of their ingredients) to be determined with high sensitivity. Finally, it can be used as a bolometer with a noise equivalent power (NEP) of 10^{-9} W for direct detection. Such an FRS bolometer is wavelength-selective and tunable by virtue of the Bragg condition. It can also be operated as a heterodyne detector

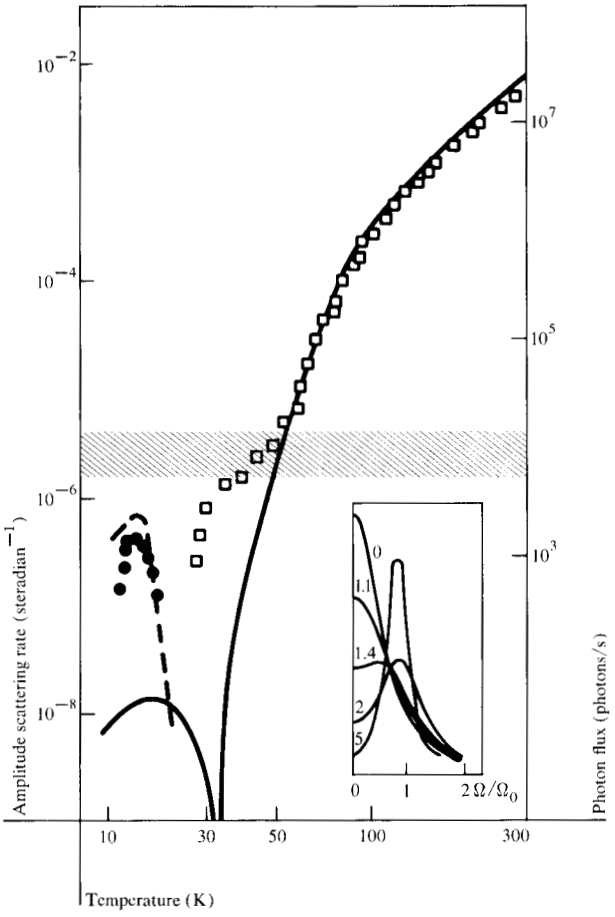

Figure 3 Forced Rayleigh scattering rate and photon flux for steady state scattering ($\Omega = 0$) (—□—) and for second sound resonance ($\Omega = \Omega_0$) (--●--). The shaded portions of the figures refer to shot noise normalized to 1-Hz bandwidth. The insert illustrates the spectral crossover from diffusive to wavelike behavior, where the numbers on the curves refer to values of Ω_0/Γ_R; see Ref. [17].

Table 1 Sensitivity of FRS (thermal gratings, typical limiting values for 1-Hz bandwidth).

Quantity	*Relation*	*Examples*	
		Solid	*Gas*
δn	$(E^s/E^{inc})/\ell k^{inc}$	10^{-13}	
$\delta\rho/\rho$	$\delta n/(\rho\partial n/\partial\rho)$	10^{-13}	
δT	$\delta n/(\partial n/\partial T)$	10^{-8} K	10^{-10} K
α	$\delta TKq^2/(I_aI_b)^{1/2}$	10^{-5} cm^{-1}	10^{-3} cm^{-1}
$(P_aP_b)^{1/2}$	$\delta TKq^2A/\alpha$	10^{-5} W	10^{-9} W
P_b	$(P_aP_b)/P_a$	10^{-10} W	10^{-18} W

(NEP = 10^{-18} W), which is of interest in the infrared regime. These high sensitivities apply to gases as sample media because of the small specific heats and thermal conductivities associated with them, and approach those of photo-acoustic techniques (spectrophony) [27].

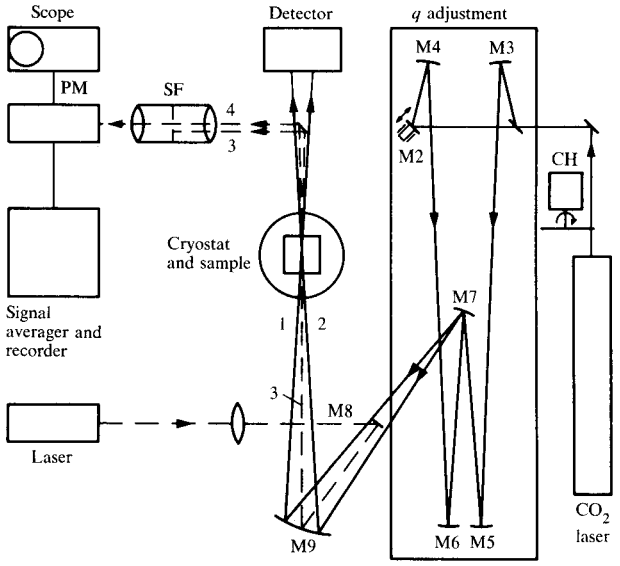

Figure 4 Experimental arrangement for FRS with infrared pumping, taken from Ref. [1].

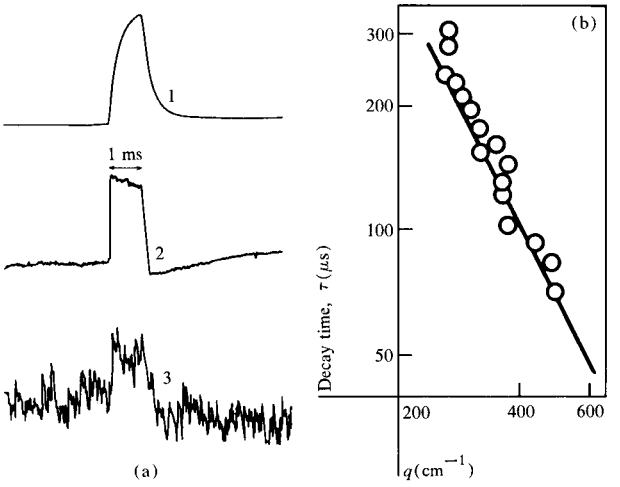

Figure 5 (a) Response to a rectangular pump pulse in NaF at 300 K (curve 1), 77 K (curve 2), and 20 K (curve 3); q = 270 cm^{-1}. (b) Decay time τ *vs* q at 300 K. Figures are taken from Ref. [1].

Experiments close to thermal equilibrium

• *FRS in NaF-second sound*

In order to verify the results of the previous section and to study the feasibility of the second-sound experiment to be described later, FRS was investigated in NaF crystals [1]. Since NaF is highly transparent in the uv, visible, and near-ir regions, a pump source in the middle ir was required; CO_2 laser radiation is well suited since $\alpha \approx 0.4$ cm^{-1} at 10.6 μm.

The experimental arrangement is shown in Fig. 4. The pump radiation is sent from a 10-W laser through the chopper CH and is split into two beams, the relative phase, orientation, and spot sizes of which are adjusted by means of mirrors M2 to M9. The arrangement allows variation of the angle between the pump beams without changing the points of intersection. The latter are in the center of the sample and, for control purposes, at M7. The somewhat involved setup greatly facilitates alignment of the ir beams. The paths of the probe and scattered beams are indicated by dashed lines. A spatial filter (SF) behind the sample selects the scattered radiation, which is detected by a photomultiplier (PM) followed by a signal averager.

The response of the scattered signal to a rectangular pump pulse of 1-ms duration is illustrated by displays from the signal averager [Fig. 5(a)]. The slow response at room temperature is clearly distinguished from the rectangular shape of the signals at 77 and 20 K. The difference is caused by the strong increase of the thermal conductivity at low temperatures [23]. At 20 K the signal is very weak and scarcely overcomes noise.

The signal was identified by its direction, dependence on I_a and I_b, phase, and decay time, which is proportional to q^{-2} [Fig. 5(b)]. The temperature dependence of the experimental data is plotted in Fig. 3, showing good agreement with the calculated values for $T > 50$ K. The indicated level of shot noise was determined experimentally. It is on the order of magnitude expected from theoretical considerations.

Second sound in solids consists essentially of a compressional wave in the phonon gas in analogy to regular sound in a regular gas [22, 23]. In order not to be overdamped, phonon collisions must be predominantly elastic. This is possible in very high quality crystals within a certain "window" of frequencies and temperatures.

Experimental verification, though challenging because of setting bounds to the law of heat diffusion, turned out to be difficult, both with respect to sample preparation and detection. Finally, strong evidence for second sound was obtained from heat pulse techniques [23]. However, an alternative method of observation that distinguishes between wavelike and other (say, solitonlike) types of propagation is desirable; FRS is well suited for this purpose.

In order to detect second sound, the experimental arrangement was slightly modified. The pump radiation was amplitude-modulated up to 10 MHz by beating two stabilized CO_2 lasers [5]; the FRS signal then carries a component with the same modulation. If second sound really were wavelike, the resonance structure of Eq. (10a) should be found near $\Omega_0 = q/c_0$.

A resonance structure does in fact appear near $\Omega/2\pi \approx$ 6.5 MHz and 20 K (Fig. 6). The relation among Ω, q, and c_0 unambiguously identifies it as second sound. The width of the resonance allowed damping of second sound to be determined for the first time.

• *Further investigations on heat transport*

Forced Rayleigh scattering was demonstrated independently by Eichler and coworkers [2] using ruby and liquids such as glycerol and methanol colored by small admixtures of a dye. An argon laser was used for excitation. Since the thermo-optic coupling is relatively strong in liquids, homodyne detection was possible and the experimental setup could be kept less sophisticated (Fig. 7). With sufficiently thin cuvettes, the sample behaves like a flat grating. Several orders of scattered light were observed.

Urbach, Hervet and Rondelez [4] investigated the anisotropy of χ in several liquid crystals by FRS. To do this by classical methods would be difficult because of the requirement for relatively large samples that cannot be kept easily in a monodomain structure. The FRS technique, however, only requires a small volume and thermal amplitude (avoiding the risk of heater-induced convection), and the time of measurement is short. A Dove prism in the path of the pump beams allowed further rotation of the grating structure with respect to liquid crystal orientation.

The largest χ was found with $\vec{q}$ parallel to the molecular axis. This behavior can be followed through different phases as a function of temperature (Fig. 8). Of particular interest are the results for a smectic C phase showing clearly that the χ anisotropy is caused by orientation of the molecular axis and not the layer structure [4].

Anomalous behavior of FRS was found in a recent investigation of glasses at low temperatures [30]. Amorphous materials are distinguished from crystals by the possibility of structural rearrangement [31]. This process may be described by the motion of a particle in a double-well potential. Fluctuations in the population of these "two-level states" are expected to influence the low-frequency scattering of light [32]. To a large extent, FRS overcomes the signal-to-background problem that

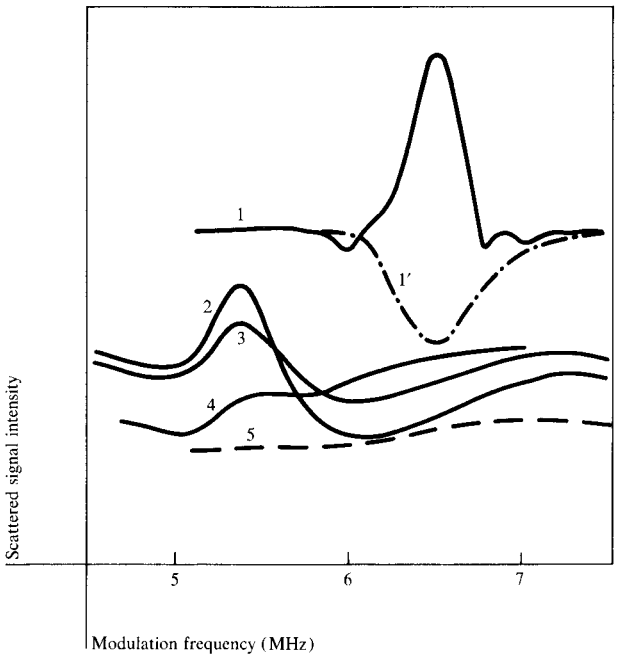

Figure 6 Forced Rayleigh scattering signals in NaF showing resonance structures at (1) 17.3, (2) 19.8, (3) 20.1, and (4) 21.5 K. Curve 5 is the control curve with the pump lasers blocked, and curve 1′ refers to a phase reversal of 180° at 17.3 K. The figure is based on one in Ref. [5].

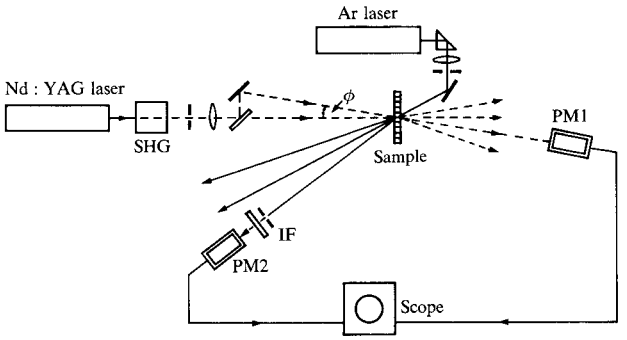

Figure 7 Experimental arrangement for FRS with thin samples and pumping with visible light [38].

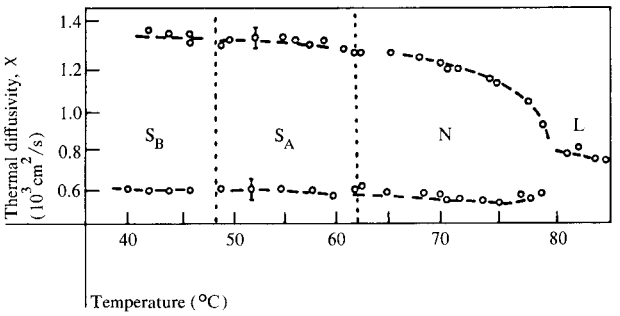

Figure 8 Anisotropic thermal diffusivity of the liquid crystal p-butoxybenzylidene-p-n-octylaniline (BBOA) [39].

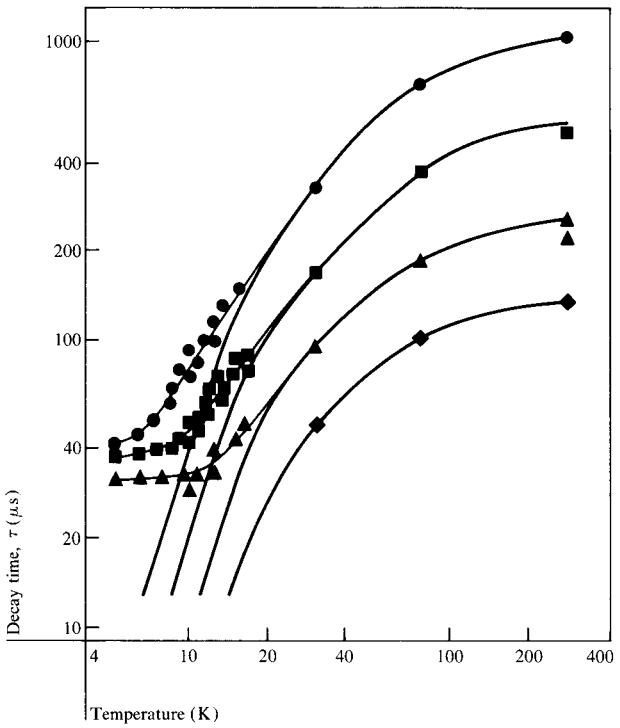

Figure 9 "Anomalous" FRS in FG18 glass; $q/2\pi$ = 72 (●), 103 (■), 144 (▲), and 206 cm^{-1} (◆); see Ref. [30].

restricted the investigation of classical Rayleigh scattering to temperatures above 60 K [33]. Optical filter glasses (Schott BG20 and FG18) were chosen as the sample materials. These were mounted on a cool finger for measurements between 25 and 300 K, and inside a pumped He^4 cryostat for measurements at lower temperatures.

Attention was focused on the variations of the coupling factor $(\partial n/\partial T)_{eff}$ and decay time τ with temperature (Fig. 9). At room temperature, $(\partial n/\partial T)_{eff}$ is on the order of 10^{-5} K^{-1}, which is typical for many glasses and crystals. Down to about 70 K, $(\partial n/\partial T)_{eff}$ strongly decays with temperature, but below this it becomes practically constant, as compared with the approximate T^3 dependence for simple crystalline materials. The extra scattering appears to be the first-time observation of an influence of rearrangement on the refractive index. At low temperatures the decay times show distinct deviations from the curves calculated for stationary values. These deviations might be caused by a finite relaxation time between two-level states and the thermal bath of phonons.

• *Investigations of mass diffusion*

The diffusion of photochromic molecules in a host material can be studied by FRS in an elegant way [34a, b]: Irradiation with a pump pulse creates an absorption grating, the decay of which is a measure of mass diffusivity χ_m. A major advantage of FRS results from the small diffusion length $2\pi/q$, which allows for quick observations even at small values of χ_m (10^{-7} to 10^{-12} cm^2/s). The anisotropic mass diffusion of methyl red in the liquid crystal p-methoxybenzylidene-p-n-butylaniline (MBBA) was studied this way, and excellent agreement with data from other techniques was found. The method was extended recently to polymer solutions containing macromolecules labeled with a photochromic group. Hervet, Leger, and Rondelez [34b] studied mass diffusion by "reptation" in these materials for the first time, using FRS.

• *Coupled modes*

A number of investigations have been made concerning the coupling between local heating and other modes. The signal from the secondary process can be easily separated from the thermal one if its characteristic time is either considerably faster or considerably slower than $\tau = 1/\chi q^2$. In the first case, the signal shows up as a delayed response to a short pump pulse, and in the latter, as a second slow decay. Cowen, Allain, and Lallemand [35] demonstrated the interaction with the so-called Mountain mode in liquids. Two characteristic times could be distinguished [Fig. 10(a)], the fast one representing the response of *forced Mountain scattering*. In a similar way, the interaction with concentration fluctuations in a mixture was demonstrated, yielding a new method for the investigation of the Soret effect [7] [Fig. 10(b)]. Note that the rearrangement of molecules responsible for the Mountain mode is a local relaxation; the fast exponential is therefore independent of q. In the case of concentration fluctuations, both decay times are proportional to q^{-2}. Chan and Pershan [6] measured the diffusion of water between smectic lipid membrane layers for the first time using FRS [Fig. 10(c)]. In their investigation, the decay time of the overall heating (finite spot-size effect) was quite close to the mass diffusion time $\tau_m = \chi_m^{-1} q^{-2}$ but could be eliminated by the periodic inversion of both the phase and signal.

A Benard cell is a flat container completely filled with a liquid that can be heated from below and cooled from the top. At a certain temperature gradient, convection sets in to form a regular flow pattern. This so-called Benard instability has many properties in common with a phase transition [36]. The question was whether temperature fluctuations coupled to velocity would critically slow down close to the transition. Allain, Cummins, and Lallemand [8] demonstrated this phenomenon in an FRS experiment by adjusting q to the flow pattern periodicity and watching the decay time upon approach to the critical gradient [Fig. 10(d)].

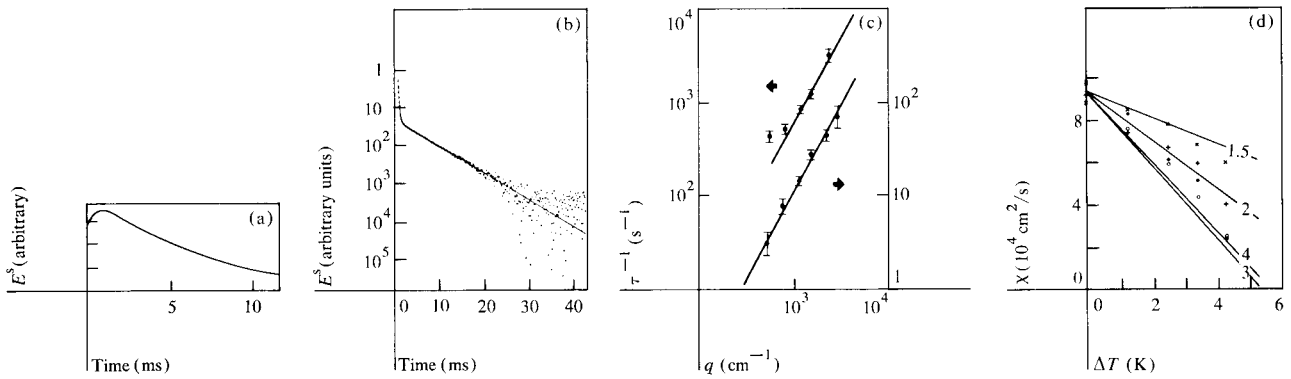

Figure 10 Forced Rayleigh scattering in (a) glycerol at 60.5°C [40] and (b) CS_2; ethanol [41]. (c) Decay times for pure thermal diffusion (left axis) and for the mixed mode (right axis) in smectic liquid membrane layers [42]. This demonstrates the q^2 dependence of the decay. (d) Critical slowing-down near the Benard instability for the wave vector values indicated [43].

Experiments far from thermal equilibrium

In general, gratings of electronic excitations are of the absorption type and quite short-lived. They decay by de-excitation or sometimes by transport. The characteristic features are similar to the "low" energy excitations previously discussed; however, a time resolution in the nanosecond to picosecond range and correspondingly increased pump and probe powers are required.

These requirements are met by the use of mode-locked or Q-switched lasers and variably delayed probe pulses. The decay time is measured in a stroboscope-like fashion, being limited only by the pulse width of the probe beam (Fig. 11). The usefulness of this technique was demonstrated by Phillion, Kuizenga, and Siegman [9], who determined the orientational relaxation times and singlet lifetimes of rhodamine 6G in various alcohols.

More recently, Salcedo *et al.* [12] studied the energy transfer of singlet excitations of pentacene in p-terphenyl. De-excitation and excited state diffusion could be distinguished by analyzing the q dependence. A similar apparatus was used by Hoffman *et al.* [14] for the measurement of surface recombination velocities in the semiconductors GaAs and InP and the ambipolar diffusion coefficient. These investigations are of particular interest because of the great technical importance of the effects involved.

Eichler, Hartig, and Knof [11] studied transient gratings in CdS using detection electronics with high time resolution instead of the delay technique. Using a mode-locked, frequency-doubled YAG laser as the pump source and a pulsed dye laser as the probe, they found decay times of approximately 6 ns; these were ascribed to the deactivation of luminescence centers.

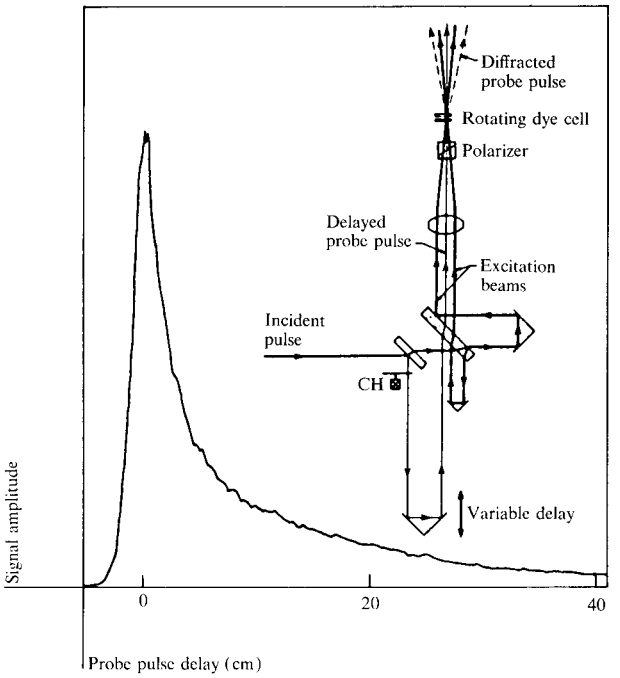

Figure 11 Schematic of transient grating apparatus and a typical exponentially decaying signal trace [44].

More details concerning FRS far from thermal equilibrium and related experiments can be found in the reviews by Eichler [37].

Outlook for future applications

It is now possible to make various crystals (apart from NaF) of high enough quality to support second sound or at least to show deviations from purely diffusive behavior that can be investigated by FRS. The technique may also find interesting application in the field of phase transitions. Coupling between energy and the order parameter may be investigated by using short pulses and high time

resolution. Melting, boiling, and decomposition may be influenced by the periodic structure of the thermal grating.

In superionic conductors, contributions to the thermal conductivity from mobile ions are likely to be seen. In a somewhat different experimental arrangement, vortex lines in type I superconductors may be ordered along the interference minima of a thermal grating and detected in reflection.

The number of nonthermal FRS mechanisms could be extended to include polaronic effects, solarization, and photochemical effects. Finally, FRS has potential for low-level absorption spectroscopy because the scattered signal amplitude is proportional to the absorption coefficient at the frequency of the pump radiation, quite small values can be measured, and surface effects can be avoided.

Acknowledgments

The author acknowledges critical reading and helpful suggestions by H. J. Eichler, Technical University of Berlin, R. Gammon, Maryland University (presently a visiting scientist at the IBM Zurich Research Laboratory), and F. Rondelez, Collège de France, Paris.

References and notes

1. D. W. Pohl, S. E. Schwarz, and V. Irniger, *Phys. Rev. Lett.* **31,** 32 (1973).
2. (a) H. Eichler, G. Salje, and H. Stahl, *J. Appl. Phys.* **44,** 5383 (1973); (b) H. Eichler, G. Enterlein, P. Glozbach, J. Munschau, and H. Stahl, *Appl. Opt.* **11,** 372 (1972).
3. D. W. Pohl, in *Proceedings of the International Conference on Lattice Dynamics*, M. Balkansky, Ed., Flammarion, Paris, 1977, p. 782.
4. (a) W. Urbach, H. Hervet, and F. Rondelez, *Mol. Cryst. Liq. Cryst.* **46,** 209 (1978); (b) F. Rondelez, W. Urbach, and H. Hervet, *Phys. Rev. Lett.* **41,** 1058 (1978).
5. D. W. Pohl and V. Irniger, *Phys. Rev. Lett.* **36,** 480 (1976).
6. (a) W. Chan and P. S. Pershan, *Phys. Rev. Lett.* **39,** 1368 (1977); (b) W. Chan and P. S. Pershan, *Biophys. J.* **23,** 427 (1978).
7. K. Thyagarajan and P. Lallemand, *Opt. Commun.* **26,** 54 (1978).
8. C. Allain, H. Z. Cummins, and P. Lallemand, *J. de Phys. Lett.* **39,** L-473 (1978).
9. D. W. Phillion, D. J. Kuizenga, and A. E. Siegman, *Appl. Phys. Lett.* **27,** 85 (1975).
10. H. J. Eichler and J. Knof, *Appl. Phys.* **13,** 209 (1977).
11. H. J. Eichler, C. Hartig, and J. Knof, *Phys. Status Solidi A* **45,** 433 (1978).
12. J. R. Salcedo, A. E. Siegman, D. D. Dlott, and M. D. Fayer, *Phys. Rev. Lett.* **41,** 131 (1978); J. R. Salcedo and A. E. Siegman, *IEEE J. Quantum Electron.* (in press).
13. F. Rondelez, H. Hervet, and W. Urbach, *Chem. Phys. Lett.* **53,** 138 (1978).
14. C. A. Hoffman, K. Jarasiunas, H. J. Gerritsen, and A. V. Nurmikko, *Appl. Phys. Lett.* **33,** 536 (1978).
15. See, *e.g.*, B. Chu, *Laser Light Scattering*, Academic Press, Inc., New York, 1974.
16. Lord Rayleigh, *London, Edinburgh and Dublin Philosophical Magazine and Journal of Science (Phil. Mag.)*, (4) **41,** 274, 447 (1871); **47,** 375 (1899).
17. A. Griffin, *Phys. Lett.* **17,** 208 (1965) and *Rev. Mod. Phys.* **40,** 167 (1968); R. A. Guyer, *Phys. Lett.* **19,** 261 (1965); R. H. Enns and R. R. Haering, *Phys. Lett.* **21,** 534 (1966).
18. D. W. Pohl, *Solid State Commun.* **23,** 447 (1977).
19. D. W. Pohl and S. E. Schwarz, *Phys. Rev. B* **7,** 2735 (1973).
20. See, *e.g.*, L. D. Landau and E. M. Lifshitz, *Statistical Physics*, Pergamon Press, Inc., London, 1958, Ch. 12.
21. See, *e.g.*, L. D. Landau and E. M. Lifshitz, *Electrodynamics of Continuous Media*, Pergamon Press, Inc., London, 1960, Ch. 14.
22. A comprehensive list of references on the extended literature on the theory of second sound is found in H. Beck, P. F. Meier, and A. Thellung, *Phys. Status Solidi A* **24,** 11 (1974), and in the experimental papers of Ref. [23].
23. H. E. Jackson and C. T. Walker, *Phys. Rev. B* **3,** 1428 (1971); T. F. McNelly, S. J. Rogers, D. J. Channin, R. J. Rollefson, W. M. Goubau, G. E. Schmidt, J. A. Krumhansl, and R. O. Pohl, *Phys. Rev. Lett.* **24,** 100 (1970).
24. I. P. Batra, R. H. Enns, and D. Pohl, *Phys. Status Solidi B* **48,** 11 (1971).
25. H. Eichler, G. Enterlein, J. Munschau, and H. Stahl, *Z. Angew. Phys.* **31,** 1 (1971).
26. R. K. Wehner and R. Klein, *Physica* **62,** 161 (1972).
27. W. Herrmann and D. W. Pohl, IBM Zurich Research Division laboratory, 8803 Rüschlikon, Switzerland (to be published).
28. A. E. Siegman, *J. Opt. Soc. Amer.* **67,** 545 (1977).
29. See, *e.g.*, M. Ross, *Laser Receivers*, John Wiley & Sons, Inc., New York, 1966.
30. D. W. Pohl and V. Irniger, *Phys. Rev. Lett.* **43,** 143 (1979).
31. See, *e.g.*, the reviews of R. O. Pohl and G. L. Salinger, *Ann. N.Y. Acad. Sci.* **279,** 150 (1976), and S. Hunklinger and W. Arnold in *Physical Acoustics*, Vol. 12, W. P. Mason and R. N. Thurston, Eds., Academic Press, Inc., New York, 1976, p. 155.
32. C. Cohen, *Phys. Rev. B* **13,** 866 (1976); J. Jaeckle and K. L. Juengst, *Z. Phys. B* **30,** 243 (1978).
33. P. A. Fleury and K. B. Lyons, *Phys. Rev. Lett.* **36,** 1188 (1976).
34. (a) H. Hervet, W. Urbach, and F. Rondelez, *J. Chem. Phys.* **68,** 2725 (1978). (b) H. Hervet, L. Leger, and F. Rondelez, *Phys. Rev. Lett.* (in press).
35. J. A. Cowen, C. Allain, and P. Lallemand, *J. de Phys. Lett.* **37,** L-313 (1976).
36. See, *e.g.*, *Fluctuations, Instabilities, and Phase Transitions*, T. Riste, Ed., Plenum Press, New York, 1975.
37. H. J. Eichler, *Opt. Acta* **24,** 631 (1977) and *Festkörperprobleme* **18,** 241 (1978).
38. Copyright 1973, American Institute of Physics, New York; reprinted with permission from Ref. [2(a)].
39. Copyright 1978, Gordon and Breach Science Publishers, Ltd., New York; reprinted with permission from Ref. [4(a)].
40. Copyright 1976, *Journal de Physiques*, Les Editions de Physique, Orsay, France; reprinted with permission from Ref. [35].
41. Copyright 1978, North-Holland Publishing Co., Amsterdam; reprinted with permission from Ref. [7].
42. Copyright 1977, American Institute of Physics, New York; reprinted with permission from Ref. [6(a)].
43. Copyright 1978, *Journal de Physiques*, Les Editions de Physique, Orsay, France; reprinted with permission from Ref. [8].
44. Copyright 1975, American Institute of Physics, New York; reprinted with permission from Ref. [9].

Received April 2, 1979

The author is with the IBM Zurich Research Division laboratory, 8803 Rüschlikon, Switzerland.